Picosecond Optics and Microwave Technology

CHI H. LEE, SENIOR MEMBER, IEEE

(*Invited Paper*)

Abstract—**Progress in the application of ultrafast optics to microwave and millimeter-wave technology using picosecond photoconductors is reviewed. The generation, control, and characterization of both pulsed and CW high-frequency waves using a frozen wave generator, an impulse excited resonator, and a spectral filter are presented. A time-domain network analyzer which uses optoelectronic techniques for on-wafer monolithic microwave and millimeter-wave integrated circuit measurements is described.**

I. INTRODUCTION

RAPID ADVANCES in both microwave and optical technologies make it possible to integrate them to form a new class of devices that can perform high-speed/high-frequency electronic functions. With the advent of femtosecond lasers, we envision such devices to work in the picosecond time domain. This new technology, which combines the fields of optics and electronics, is referred to as picosecond optical electronics. The link for these two fields is picosecond photoconductivity.

The ideas of using the photoconductivity effect for the control of microwave solid-state devices have been of great interest to the microwave community recently. For example, optical control of IMPATT [1]–[3], TRAPATT [4], MESFET [5], [6], transferred-electron devices [7], and HEMT [8] has been reported. Microwave signal generation at 35 GHz by optical mixing of injection locked laser diode sources [9] and indirect optical locking of a free-running 39 GHz IMPATT oscillator [10] have been demonstrated. The application of injection locked oscillators for optically fed phased array antennas has been reported [11]. The basic operation principle of all these devices is the photogeneration of free electron–hole pairs within the active region of a device. Photoexcited carriers modulate transconductance and other circuit parameters (such as gate–source and drain–gate capacitances) of the devices. Therefore, optical illumination will either enhance or quench the oscillation of these devices.

The optical technique for controlling microwave devices offers unique advantages in: (1) near perfect isolation between controlling and controlled devices, (2) elimination of RF feed in a large array system, (3) immunity from electromagnetic interference, (4) light weight and compact size, (5) extremely fast response, (6) high power handling capability, and (7) possibilities for monolithic integration. In the references mentioned above, the extreme high speed capability of the lightwave technologies has not been exploited.

In our laboratory, we have taken advantage of the unique speed capability of the optical pulses. Electrical pulses are instantaneously generated via the picosecond photoconductivity [12] effect in a photoconductor. Picosecond photoconductors can now be engineered to generate electric pulses as short as 1 ps [13] with jitter-free switching. All subsequent electronic events can be slaved to this initial pulse. Picosecond optical techniques can be utilized again to generate other pulses that can be precisely time controlled. Using picosecond optical electronic techniques, we are able to generate microwave and millimeter-wave signals that are in complete time synchronization with the exciting optical pulses. RF waveform generation, ranging from one monocycle [14] to continuous wave, with peak power up to a few megawatts in the pulsed case and frequency up to 20 GHz in the CW case [15], has been achieved. Phase control of the microwave signals can be accomplished by simply controlling the arrival time of the exciting optical pulses which offers the potential for a true time delay phased array radiation.

I will review the progress in the application of ultrafast optics to microwave and millimeter-wave technology through picosecond optoelectronics. The term *picosecond optoelectronics* is defined as an electronic function performed by picosecond optical pulses via the photoconductivity effect.

Since most of the works reviewed here involve the use of picosecond photoconductors, I will begin by summarizing the characteristics of picosecond photoconductors in the next section. This will be followed by a discussion of the principle of optical generation and control of microwave pulses in Section III. Sequential RF waveform generation using a frozen wave generator and picosecond photoconductive switch is discussed in Section IV. Impulse excitation of a resonant coaxial cavity to generate microwave reviewed in Section V. Section VI deals with CW

Manuscript received August 7, 1989; revised November 16, 1989. This work was supported by the U.S. Army Research Office, the Air Force Office of Scientific Research, and the National Science Foundation.

The author is with the Department of Electrical Engineering, University of Maryland, College Park, MD 20742

IEEE Log Number 8934044.

0018-9480/90/0500-0596$01.00

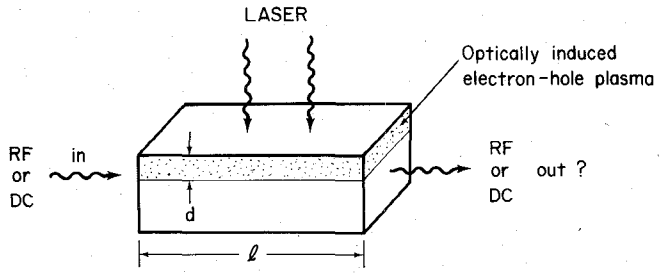

Fig. 1. Interaction of low-frequency electromagnetic waves with the photoinduced electron–hole plasma in a semiconductor; d is the penetration depth of the optical beam. For a weakly absorbing medium, d may be greater than the thickness of the sample.

microwave generation by ultrafast optical technique. On-wafer optoelectronic characterization of monolithic millimeter-wave integrated circuits is discussed in Section VII. Concluding remarks and prospects for future development of this field can be found in the last section.

II. Picosecond Photoconductors

A photoconductor exhibiting picosecond response time is referred to as a picosecond photoconductor. This phenomenon is referred to as the picosecond photoconductivity effect and was first reported in 1972 [12]. Picosecond photoconductors used as ultrafast switching and gating devices have been demonstrated. In this application, the photoconductor is dc biased at the input terminal and a fast rise electrical output signal is obtained instantaneously when it is irradiated by a picosecond optical pulse. Thus, in a sense, it is a three-terminal device where the control terminal is an optical port.

There are a large number of devices based on the picosecond photoconductivity effect. They include switches, gates, samplers, electronic impulse function correlators, A/D converters, optical detectors, dc to RF converters, and coherent microwave generators. The principle of operation for some of these devices will be discussed in this paper. They are mostly based on the interaction of electromagnetic waves with photoinduced electron–hole pairs in a bulk semiconductor. Recently a number of photoconductive devices using semiconductor films have been reported [16], [17].

Let us consider the interaction of an RF signal (including dc signal) with an electron–hole plasma in the semiconductor as shown in Fig. 1. The electron–hole plasma in the layer with thickness d introduces complex permittivity in the plasma region, which can be expressed as

$$\epsilon_r = \epsilon' - j\epsilon'' \tag{1}$$

$$= \epsilon_L - \frac{\omega_p^2}{\omega^2 + \nu^2} - j\frac{\nu}{\omega}\frac{\omega_p^2}{\omega^2 + \nu^2} \tag{2}$$

where ω is the angular frequency of the RF field; ϵ_L is the dielectric constant of the host lattice; ν is the carrier collision frequency; and ω_p is the plasma frequency, given by

$$\omega_p = ne^2/\epsilon_0 m^*. \tag{3}$$

Here n is the density of the photoinduced excess carriers proportional to laser intensity, e is the electronic charge, m^* the effective mass, and ϵ_0 the permittivity of vacuum. In the case of a low-frequency RF signal $\omega \ll \nu$, $\omega_p \ll \nu$ (for frequency below X-band), the photoinduced carrier will not affect the real part of the complex permittivity, and the effective conductivity

$$\sigma_{\text{eff}} = \omega\epsilon_0\epsilon'' = ne\mu \tag{4}$$

where μ is the mobility. However, for a high-frequency RF signal (such as millimeter waves in the 30–100 GHz range), the effect of photoinduced plasma on the real part of the permittivity can no longer be neglected. The photoinduced plasma will cause refractive index change for the RF signal, effectively making also phase modulation on the propagating RF signal. The plasma state in a semiconductor therefore provides us with a flexible situation for the switching and controlling of an electromagnetic signal in a conductive as well as in a dielectric mode of operation. In a conductive mode device, the wavelength of the RF signal to be controlled or generated is usually much greater than the physical dimensions of the solid-state plasma region; thus the plasma region can be considered a lumped circuit element. In a dielectric mode device (such as a millimeter-wave phase shifter) the wavelength of the propagating RF signal is comparable to the dimensions of the plasma region; therefore the plasma region is considered a distributed circuit element. The dielectron mode device has been reviewed previously [18], [19] and will not be discussed here.

III. Conductive Mode Devices Based on Photoconductive Switches

Most of the applications of picosecond photoconductors are conductive mode devices based on photoconductive switches. The actual design of the switch depends on the specific application. The switch is a bulk device which can be scaled in size. For high-frequency, high-speed applications, the output voltage requirement is low; thus the photoconductive gap length is typically of the order of a few micrometers. For high-power switches, however, the device size is usually in millimeters or even centimeters. Fig. 2 shows some of the typical designs. In the microstrip category, the photoconductor can be straight gap or interdigitated to have more area for optical illumination to increase optical efficiency. However, the time response of the interdigitated switch may suffer because of the increased length of the electrode–semiconductor interface. To achieve extreme speed one has to use the coplanar microstrip design to reduce the circuit capacitance to a minimum. Electric pulses of 350 fs duration have been generated with this new design [20].

In order to preserve the inherent bandwidth capability of the picosecond photoconductive device, the photoconductor is used as a switch in a charged transmission line pulser arrangement (Fig. 3). In this arrangement the charging segment of the transmission line is attached to one electrode of the photoconductive switch at one end of the

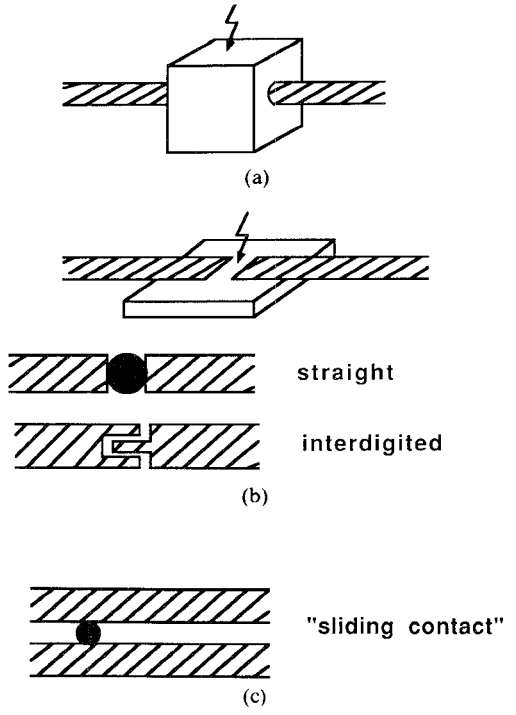

Fig. 2. Different photoconductive switch designs: (a) Bulk switch for high-power application (b) 50 Ω microstrip design for low-power, high-speed application; the gap can be straight gap or interdigitated. (c) Coplanar striplines for very high speed applications

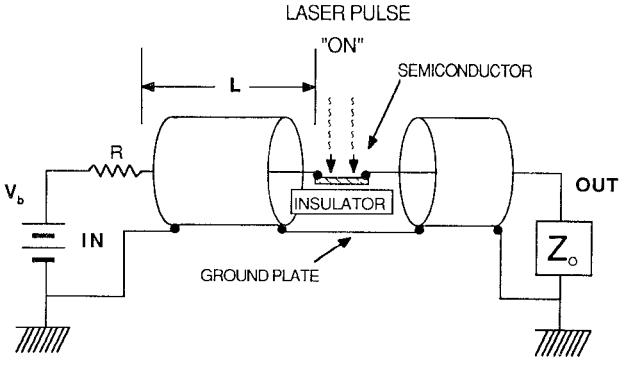

Fig. 3. Charged line pulser arrangement with a photoconductive switch. The charged line length is L and the characteristic impedance of the line is Z_0. R is the charging resistor and the output line is terminated with a matched load Z_0.

segment and is connected to the charging voltage source at the other end. The output end of the switch is connected to the output line which is terminated by a matched load. In order to achieve good isolation between the input and output, the photoconductive materials chosen always have high dark resistivity. Table I shows some of the picosecond photoconductors. Note the high dark resistivity of all materials. Among them silicon has the lowest dark resistivity, resulting in a serious thermal runaway problem.

The high dark resistivity of the switch makes it nonconductive in the dark state. Assuming that picosecond or femtosecond optical pulses are illuminating the photoconductor and are being absorbed by the material, electron–hole pairs will be created instantaneously, transforming the photoconductor from an insulating to a conducting

TABLE I
SEMICONDUCTOR MATERIALS INVESTIGATED FOR HIGH-SPEED, HIGH-POWER PHOTOCONDUCTIVE SWITCHING

Semiconductor	Eg (ev)	Carrier Lifetime (ns)	Dark Resistivity (Ω-cm)
Si (intrinsic)	1.16	10^4	5×10^4
SoS		10 ~ 1 ps	
*Cr:GaAs	1.42	< 1	$>10^7$
Fe:InP	1 29	< 1	$>10^7$
*CdS_xSe_{1-x}	1.8 ~ 2.4	> 10	$> 10^7$
GaP	2.24	> 1	$> 10^7$
*(Diamond (IIa))	5.5	< 1	$> 10^{16}$
Fe:In:GaAs		500 ~ 100 ps	
GaAs on SoS		20 ps	

*First developed at the University of Maryland

state and thus closing the switch. The fast rise electrical pulse will appear at the load, with the rise time of the electrical pulse approaching that of the laser pulse. The actual shape of the electric pulse depends on the duration of the time that the switch remains closed. This time is usually referred to as the photoconductive lifetime, and it has two contributions: carrier recombination time and swept out time. In the case where the photoconductive lifetime, τ, is much greater than the round-trip propagation time of the voltage wave on the charged line section, $2L/v$, one expects a square waveform to appear at the load with its rise and fall times equal to the rise time of the laser pulse. Here L is the length of the charged line segment and v is the velocity of the voltage wave propagating on the line. If $\tau \ll 2L/v$, one expects to see a single-sided exponential waveform. Here again the rise time of the pulse is equal to that of the laser pulse but the fall time reflects the photoconductive decay time (assuming that the switch is not saturated). The output voltage V_{out} is given by

$$V_{\text{out}} = V_c \frac{Z_0}{2Z_0 + R_s(t)} \tag{5}$$

where V_c is the bias or charging voltage, Z_0 is the characteristic impedance of the transmission line, and

$$R_s(t) = l_{\text{gap}}^2 / N(t)\, e\mu + R_c \tag{6}$$

is the dynamic resistance of the switch under laser illumination. Here l_{gap} is the gap length of the switch, $N(t)$ is the total number of photoinduced charge carriers (which is proportional to the optical energy of the pulse), and R_c is

the total contact resistance at the electrodes of the switch. The temporal dependence of $N(t)$ reflects the dynamics of carrier decay. When the photoconductor is used as a high-power switch, one usually requires the switch to transfer energy efficiently to the load and wants $R_s \ll Z_0$. This must be done with high biased voltage across the switch for high-power applications. The maximum hold-off voltage is

$$V_{\max} = l_{\text{gap}} E_{\text{Br}} \tag{7}$$

where E_{Br} is the intrinsic breakdown field. It is obvious from these expressions that in order to have an efficient high-power switch one requires a large l_{gap} and a high $N(t)$, i.e., large optical energy. Switches as large as a few centimeters with 100 kV of hold-off voltage strength have been fabricated in pulse power applications. The large optical energy requirement for high-power switches can be greatly reduced via a "lock-on" phenomenon [21]. High-power pulsed microwaves in the megawatt power range have been generated in our laboratory. Some of these results will be discussed later in this paper.

In contrast to high-power switches, picosecond photoconductors can also be used as high-speed optical detectors and optical electronic samplers. In general, in these applications the speed of the devices is of primary concern. The efficiency of the switch can be somewhat sacrificed. One no longer requires $R_s(t)$ to be smaller than Z_0. In fact, to maintain a linear relationship between V_{out} and the laser intensity, one needs $R_s(t) \gg Z_0$. Since high voltage output is also not required, one usually uses a small gap switch for high-speed applications. The rise time of the output electric waveform is that of the laser pulse, and the fall time of the photoconductor can be engineered to be less than 1 ps (with femtosecond laser pulse) by ion bombardment or by low-temperature MBE growth [16]. The most important characteristic of the picosecond photoconductive switch is jitter-free response. It allows perfect time synchronization between the generated electric signals and exciting optical pulses. This property holds true for both low-power and high-power switches. Many electronic and microwave functions can be time synchronized by a single optical pulse, leading to a true time delay phase arrayed system possibility. The complete time synchronization capability of this general class of photoconductive devices also gives rise to exciting and probing (or generating and sampling) techniques for on-wafer measurement of monolithically integrated millimeter-wave or high-speed digital circuits. This will be discussed later in the paper.

Practical applications of conductive mode devices include the generation of pulsed and CW microwaves via direct dc to RF conversion using picosecond photoconductive switches. To generate microwaves with a small number of cycles, a frozen wave generator has been employed. Impulse excitation of a resonant microwave cavity is used to generate microwaves with a large number of cycles. Repetitive impulse excitation can be used to generate CW microwaves. These techniques will be described in the following sections.

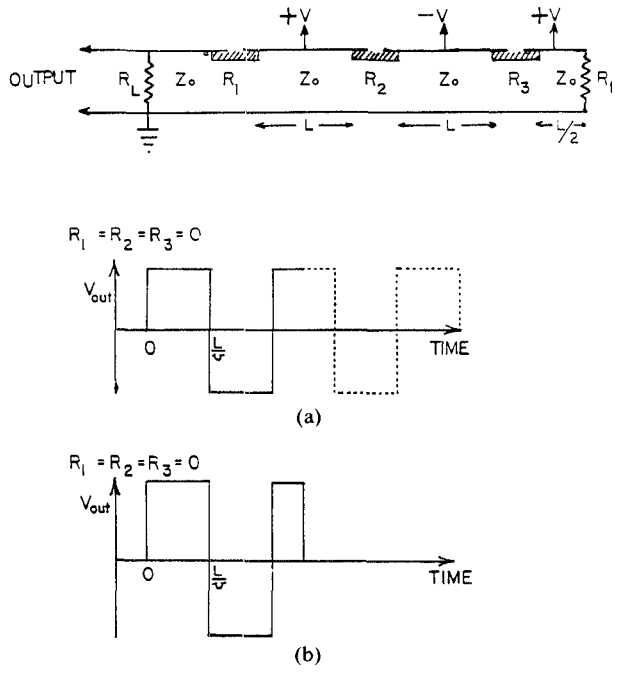

Fig. 4 Plot of waveforms generated from a frozen wave pulse generator when three switches are closed in the ideal case for (a) $R(t) = \infty$ and (b) $R(t) = Z_0$.

IV. Frozen Wave Generator

Short pulse signal microwaves have several applications such as high-resolution radar, time-domain metrology, and plasma diagnosis. A sequence of RF pulses can be generated from a dc source through a series of step recovery diodes with a rise time of 60 ps, although its pulse amplitude is limited [22]. A frozen wave generator, a simple and effective device consisting of several segments of transmission line connected in series by means of switches, is capable of generating a sequential waveform of arbitrary temporal characteristics. Proud and Norman [23] have shown the generation of a pulsed microwave signal by utilizing this frozen wave structure with nanosecond optical pulses illuminating the photoconductive switches. With nanosecond laser pulses, the advantage offered by the ultrafast response time of the photoconductive switch is not fully utilized. Hence we have designed an experiment using picosecond laser pulses to actuate the frozen wave generator, producing unique broad-band microwave pulses [24]. Fig. 4 shows a frozen wave generator with three switches and three segments of transmission lines. The last segment was designed to have a length equal to half that in the two previous segments. The end termination was left open. Here the three segments of transmission lines were charged to V_0, $-V_0$, and V_0, respectively. In the ideal case when all three switches are closed simultaneously, square pulses of two and one half cycles will be generated; the amplitude of the pulse is the same as that in the charged line structure ($V_0/2$), and the pulse width is equal to the time required for the wave to travel across one segment of charging cable of length L.

The series connection of the photoconductive switches requires that to obtain the maximum power generating

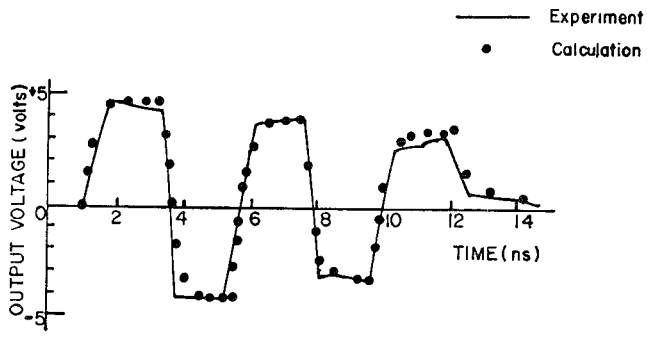

Fig 5. Plot of the experimental (solid curve) and computer simulated (dotted curve) waveform from a frozen wave generator: dc bias voltages are 10, −10, and 10 V. $L_1 = L_2 = 42$ cm, $L_3 = 21$ cm, $R_1 = 6.5\ \Omega$, $R_2 = 5\ \Omega$, and $R_3 = 7\ \Omega$.

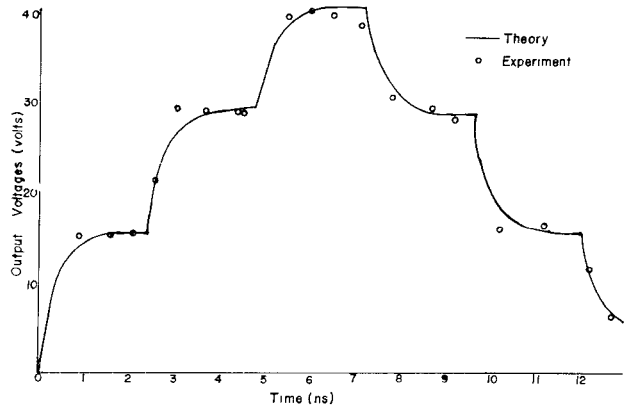

Fig 6. Stair-step waveform generated from a frozen wave generator with dc bias voltages of 35, 68 and 100 V and $L_1 = L_2 = 50$ cm and $L_3 = 25$ cm.

efficiency the switch must remain completely saturated for the entire duration during pulse forming. This means that silicon switches are preferred because of their long photoconductive lifetime. Jitters in the switching process produce random frequency modulation, which removes the energy from the fundamental frequency. Picosecond laser activated semiconductor switches seem ideal for this application since they are jitter free.

A. Symmetric Waveform Generation

For low dc bias voltage applications the frozen wave generator was mounted on a translational stage, and 10 V, −10 V, 10 V dc biases were initially applied to the three semirigid charging cables, respectively. The rise time and the fall time of the oscilloscope were both about 1 ns; therefore, the period of the output pulses was designed to be 4 ns (corresponding to that of a cable length of 84 cm). When the single laser pulse of total energy 65 μJ triggered all the switches simultaneously, a two and one half cycle wave was generated with a 4 ns period (Fig. 5). The amplitude of the first pulse was about 95% of the half bias voltage, and the total output power of these two and one half cycle pulses was about 65% of the total output power in an ideal case.

According to theory, the maximum amplitude of the output waveform should be equal to one half of the charging voltage if the on-state resistance of three switches is equal to zero. In reality, none of these resistances become zero, resulting in a reduced amplitude. By using parameters of 6.5 Ω, 5 Ω, and 7 Ω as the total resistance for three switches in the on-state and modeling the oscilloscope as a first-order low-pass filter with a bandwidth of 600 MHz, we found that the output waveform from the calculation was in agreement with the experimental results. These results are shown in Fig. 5. The dotted curve is the calculated curve and the solid line is the experimental curve.

B. Asymmetric Waveform Generation

The termination attached to the last charged line segment (opened, or matched) plays an important role in the shape and the number of cycles of the output waveform. The length of the coaxial cable and the dc bias voltage (includes the polarity) also affect the shape of the output waveform. Hence, not only the frozen wave pulse generator can provide the capability to produce symmetric waveform; other waveforms, such as asymmetrical and stair steps, can also be obtained through different arrangements. For example, in an experiment, three switches were biased with positive dc 35 V, 68 V, and 100 V, respectively, and three cables of lengths 50 cm, 50 cm, and 25 cm were utilized, with an open end termination. A stair-step waveform of 2.4 ns in separation was therefore generated (see Fig. 6). Simulation results from SPICE 2 program (solid curve) are also shown in the same figure. A series of results from six different arrangements are shown in Fig. 7. In Fig. 7(a) and (b) three cables were 50 cm, 50 cm, and 25 cm long, and three different bias voltages were applied. In parts (c), (d), and (e) of the figure, the three cable lengths were 50 cm, 50 cm, and 71 cm, respectively, and three different positive bias voltages were charged to three segments of the transmission line. In Fig. 7(f) the three cables were 50 cm, 71 cm, and 25 cm in length, and the three bias voltages were 8 V, −7.5 V, and 7.3 V, respectively. Note that Fig. 7(e) represents the character 101101.

C. Kilovolt Waveform Generation

For high-voltage applications, to prevent thermal runaway we applied a pulsed bias to three silicon switches and the wider gap switches were used for voltage hold-off. It was essential in the pulsed bias case that the bias pulse be in time synchronization with the optical pulse. Three switches were coated with clear epoxy which makes it possible to increase the pulse charging voltage to +900 V. Notice that in this situation, the center and the last switch was biased 1800 V (electric field $> 4 \times 10^4$ V/cm) across the gap. A single picosecond laser pulse of total energy ~ 50 μJ was used to activate the three switches simultaneously. The resultant output waveform, as shown in Fig. 8, has a pulse of two and one half cycles (200 MHz), a period of 4.8 ns, and an amplitude of 850 V_{p-p}.

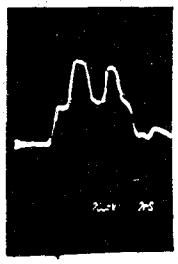

(a) dc bias of 14, 35, and 16 volts on three switches, three cable lengths of 50cm, 50cm, and 25cm. Output voltages are 200 mv/div., 12.5x attenuation, and 2ns/div., reduced scan

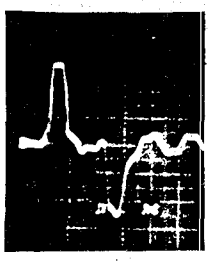

(b) dc bias of 13.6, 0.0, and 0.0 volts on three switches , three cable lengths of 50cm, 50cm, and 25cm. Output voltages are 1v/div., 2 ns/div., reduce scan.

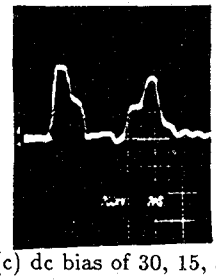

(c) dc bias of 30, 15, and 0.0 volts on three switches, three cable lengths of 50cm, 50cm, and 71cm. Output voltages are 200mv/div., 12.5x attenuation, 2ns/div., reduced scan.

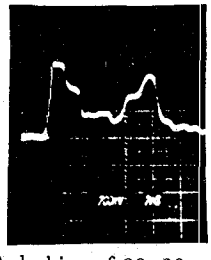

(d) dc bias of 30, 20,and 18.6 volts on three switches, three cable lengths of 50cm, 50cm, and 71cm.Output voltages are 200mv/div., 12.5x attenuation, 2ns/div., reduced scan.

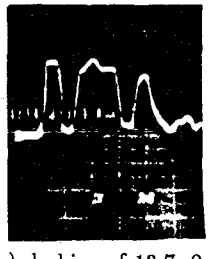

(e) dc bias of 13.7, 0.0, and 14 volts on three switches, three cable lengths of 50cm, 50m, and 71cm. Output voltages are 1v/div., 2ns/div., reduced scan.

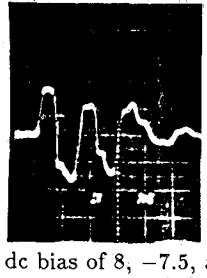

(f) dc bias of 8, −7.5, and 7.3 volts on three switches, cable lengths of 50cm. 50cm, and 71cm. Output voltages are 1v/div., 2ns/div., reduced scan.

Fig. 7. Plots of various waveforms from a frozen wave generator.

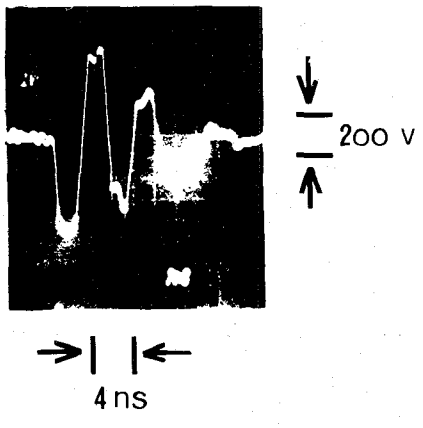

Fig. 8. Oscilloscope trace of the high-voltage waveform generated from a frozen wave generator. Pulsed bias of −900, 900, and −900 V were applied to the three switches. The three cable lengths were 50 cm, 50 cm, and 25 cm.

We have demonstrated a method of generating kilovolt and a periodic waveform by applying pulsed bias and dc bias to a frozen wave generator. This method may possibly generate sequential waveforms with higher voltages if the surfaces of the silicon switches are properly protected. However, the pulsed bias which is applied across the silicon switch can extend only to the limit set by the intrinsic bulk breakdown ($\sim 2\times10^5$ V/cm). This suggests, therefore, that in future experiments, a design utilizing switches with wider gaps will be necessary for the generation of multikilovolt sequential waveforms.

V. Direct dc to RF Conversion by Impulse Excitation of a Resonant Cavity

The frozen wave generator described in the previous section is ideal for generating RF waveforms with a small number of cycles since in the configuration shown in Fig. 4 the number of switches needed is directly proportional to

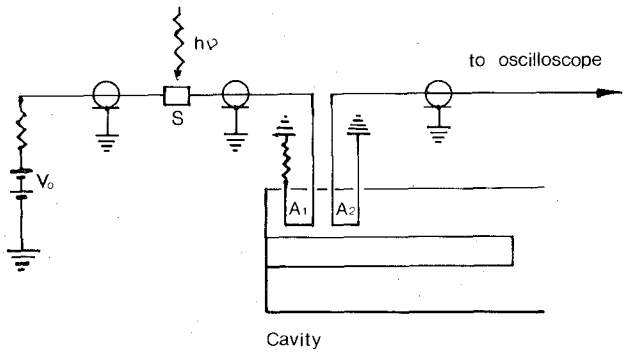

Fig. 9. Experimental arrangement for direct dc to RF conversion by impulse excitation of a resonant cavity. S is the photoconductive switch, V_0 is the bias voltage, A_1 and A_2 are input and output loop antennas, and the cavity is a coaxial structure.

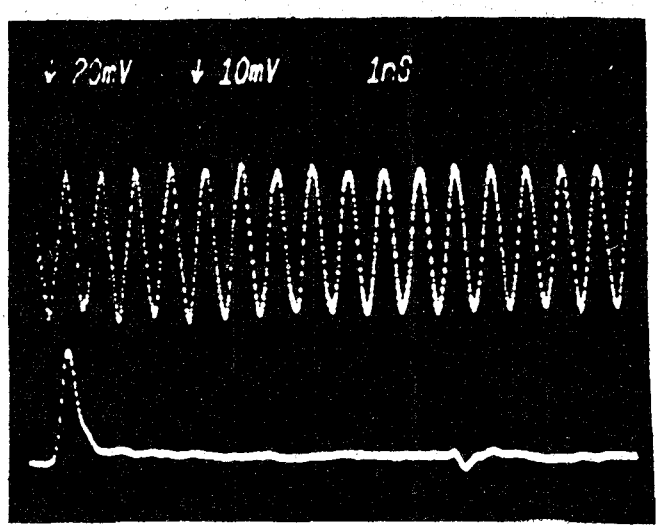

Fig. 10. The upper trace shows the CW 1.6 GHz RF signal generated from a CW mode-locked laser. The lower trace shows one of the mode-locked laser pulses from the pulse train. Note that the amplitude of the CW microwave signal remains nearly constant.

the number of cycles one needs to generate. The drawback of a frozen wave generator is that, to form an RF waveform with many periods, a large number of switches are required. These switches must be simultaneously activated and each switch must operate at close to 100% switching efficiency in order to form a good pulse sequence. This requirement naturally demands a large amount of laser energy. One of the alternatives to generating an RF waveform with many cycles is to form it in a resonant cavity with a single photoconductive switch. Pulsed microwaves with central frequency ranging from 300 MHz to 6.7 GHz have been generated by this technique. Fig. 9 shows the experimental setup, which consists of a pulsed charging line with biased voltage V_0 applied to it through a charging resistor, a photoconductive switch, which was triggered by a picosecond laser pulse, and a quarter-wavelength resonator with input and output coupling loop A_1 and A_2 respectively. The shorted and opened ends of the coaxial resonator acted as perfect reflectors for the propagating wave induced on the coaxial line. This wave would then bounce back and forth on the coaxial line, resulting in a series of pulses with alternating polarities since the boundary condition required that the voltage be zero at the shorted end and that the current be zero at the opened end. The output antenna loop A_2 was used to couple these pulses out for observation. The number of pulses generated depends on the strength of the coupling. A single dipolar microwave waveform has been generated when the coupling between the input and output loops was the strongest [14]. Near CW microwave oscillation was observed with weak coupling (Fig. 10). The frequency of oscillation was determined by the length of the cavity, and for clean oscillation the width of the input electric pulse had to be much less than the transit time of the wave propagating on the coaxial line. To obtain near CW oscillation as shown in Fig. 10 the cavity needs to be repetitively excited. To obtain an oscillation with near constant amplitude it was necessary to (1) tune the length of the coaxial cavity to an integer multiple of the repetition frequency of the laser (16 times for the data shown), (2) match the length of the transmission line between the photoconductive switch and the input antenna with that of the laser cavity, and (3) obtain a high Q for the cavity by reducing the coupling between the input and output.

We have demonstrated the conversion of dc to RF energy in a coaxial resonator by this technique. This approach has been shown to be an alternative to the frozen wave generator. Broad-band microwave pulses with over 7 kW of peak power have also been demonstrated. A detailed discussion of this work is described in [14]. To extend this approach to higher frequency a coaxial resonator with short cavity length must be used. A 6.7 GHz generator has been reported with a monolithic device using a lateral p-i-n diode as a switch. The reader is referred to [25] for details.

VI. CW Millimeter-Wave Generators

The generation of microwaves by impulse excitation of a resonant cavity is essentially waveform synthesizing by time multiplexing the short electrical pulses in a coaxial cavity. To extend this technique to millimeter-wave generation is difficult because one needs to scale the dimension of the coaxial resonator down accordingly. A simpler way to produce CW millimeter waves by the picosecond optoelectronic technique is to work in the frequency domain. As mentioned previously the output of the CW mode-locked laser is a periodic optical pulse train with interpulse spacing equal to the optical cavity round-trip time. In the laser used in our experiment this time was 10 ns. One can convert the optical pulse train to an electric one.

As schematically shown in Fig. 11, the periodic signal in the time domain contain harmonics in the frequency domain according to Fourier theory. The interharmonic spacing is equal to the reciprocal of the time spacing between two adjacent pulses. In our case it was 100 MHz, the longitudinal mode spacing from the laser used in the experiment. To obtain CW sinusoidal oscillation one simply needs to pass the periodic signal through a narrow-band filter which filters out only a single harmonic. The harmon-

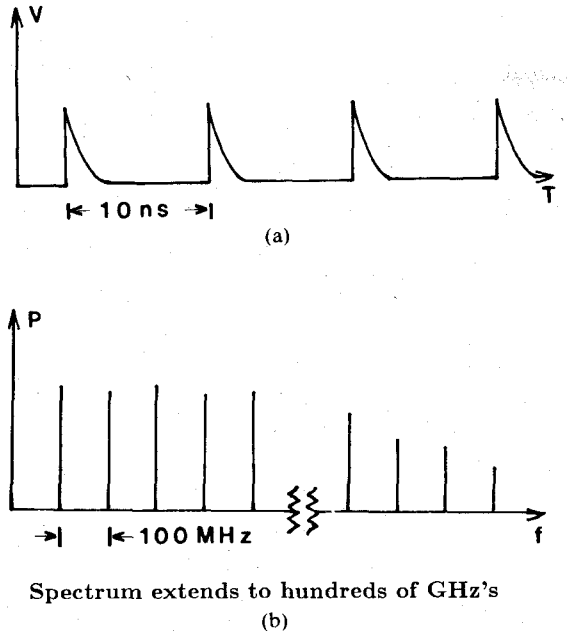

Fig. 11. Schematic showing (a) the periodic electrical pulse train generated from a picosecond photoconductor by a CW mode-locked laser and (b) the corresponding spectral components with 100 MHz spacing, extending possibly to hundreds of GHz.

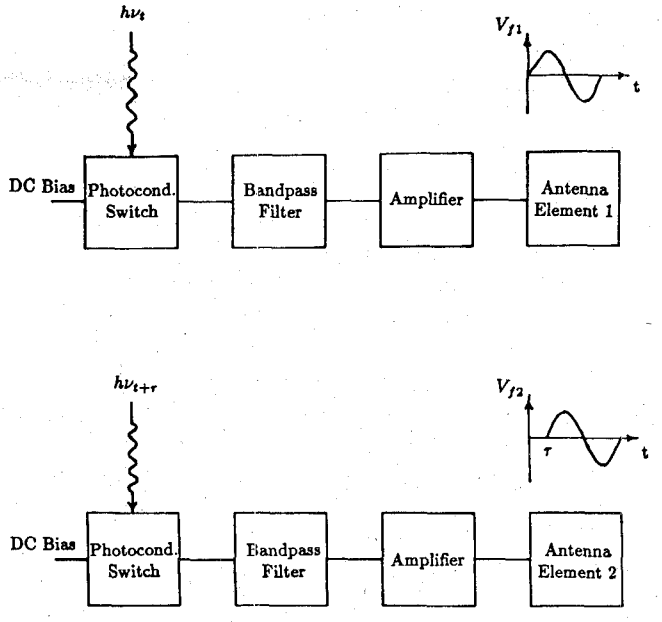

Fig. 12. Top channel is the experimental setup for 20 GHz CW microwave generators. The narrow band-pass filter selects only a single spectral component for amplification. The figure shows only two channels of a multichannel phased array antenna concept using the picosecond optoelectronic microwave source. The onset of oscillation of one channel with respect to that of the other can be precisely controlled by the arrival time of the picosecond optical pulse at the photoconductive switch.

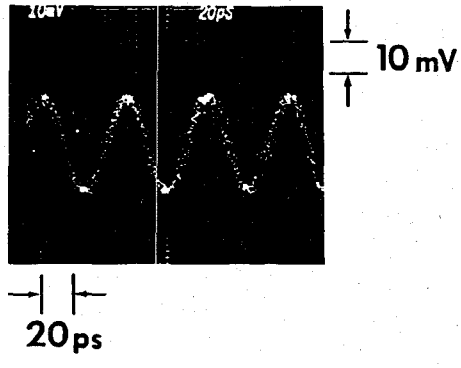

Fig. 13. Sampling oscilloscope trace of the CW 19.76 GHz signal.

ics extend to frequencies equal to the reciprocal of the individual pulse width. In order to have a flat frequency spectrum extending to 100 GHz the individual electrical pulse width needs to be less than 10 ps. Since electric pulses shorter than 1 ps have been reported, there is no problem in obtaining frequency components as high as terahertz. Since the spectral distribution is nearly uniform, for a given total power per pulse, the power per harmonic will be proportionally reduced if the bandwidth of the pulse is large. As the CW power is related to the power associated with the harmonic component, it is clear that the optimum pulse width of the input pulse should be close to the reciprocal of the carrier frequency desired. In other words the ideal pulse duration for generating CW microwaves in the 20 ~ 100 GHz range will be in the tens of picoseconds. Shorter pulses are not desirable. This is a clear case that shorter is not always better.

To generate 20 GHz CW millimeter waves we used the setup depicted in Fig. 12. The laser source consisted of a mode-locked Nd:YAG laser which was pulse compressed using an optical fiber delay line and grating arrangement, then frequency doubled using a KTP crystal. This resulted in a 532 nm wavelength and a 100 MHz pulse repetition rate with pulses which had 5 ps FWHM (full width half maximum) and an average power of approximately 200 mW, or an energy of 2 nJ in each pulse, at the switch. The bias on the photoconductor was 30 V for this experiment. When the optical signal was applied to the gap, a train of electrical pulses was produced, resulting in a spectrum with discrete signals at 100 MHz intervals. The spectral envelope was fairly flat, with gradually decreasing amplitude at the higher harmonics. The photoconductive switch used was a silicon on sapphire (SOS) microstrip structure with a simple 5 μm gap. Silicon was damaged by ion bombardment.

The output of the switch was fed to a circular waveguide dual-cavity four-pole elliptic band-pass filter, to filter the 20 GHz spectral component. The output from the filter was quite small, so a 21 dB gain GaAs MESFET amplifier designed at COMSAT was used. With the 30 V bias and using a laser power of 200 mW, the power level of the 20 GHz component at the output of the amplifier was -16 dBm. The sampling oscilloscope picture of the 20 GHz signal is shown in Fig. 13. The time jitter measured was 1.4 ps. The measured results presented here for the temporal form and time jitter of a 20 GHz signal indicate that this optoelectronic source indeed provides a low noise signal. The measured noise is primarily due to the laser, so

at present the noise process in the switch itself has not been characterized. With a stabilized laser the jitter time has been reported to decrease to less than 0.3 ps [26].

One application of this source is a millimeter-wave phased array antenna of the type shown in Fig. 12. If the optoelectronic source described is integrated into each antenna patch for the transmission operation, then only a dc signal and the optical signal need to be delivered to the patches. This offers a dramatic simplification in the feed network and hence potentially reduced cost. The principle of operation is quite straightforward. The relative patch current phase can be controlled by the relative switch excitation times. The feed network would then consist of either an optical fiber or space fed optical system and a dc bias. It is feasible to obtain high performance, as one can take advantage of high-speed optoelectronic technology.

VII. On-Wafer Optoelectronic Characterization of Monolithic Millimeter-Wave Integrated Circuits

Microwave measurements are traditionally performed in the frequency domain, where desired results are typically expressed in the form of scattering parameters. Circuit components are usually mounted in a 50 Ω microstrip network and the measurements performed with a network analyzer, such as the HP 8510. In GaAs monolithic microwave and millimeter-wave integrated circuit (MMIC) manufacture, it is desirable to be able to characterize the devices before the wafer is diced, i.e., to perform on-wafer measurements. This is possible using an external source with coplanar waveguide probes, which are customized to fit the particular integrated circuit being tested. Such mechanical contacting probes have a fairly short lifetime and deteriorating electrical performance at the higher frequencies.

In an effort to reduce the cost of large-scale on-wafer measurements and to achieve a more diverse technique, the use of optoelectronic techniques has been proposed. Several approaches for making these measurements have been studied. Frequency-domain measurements have been performed by electro-optic probing of the electrical signal on a microstrip line [26]. This work used a coplanar waveguide probe to launch the microwave signal. An alternative is to generate a very short electrical signal on-wafer by illuminating a biased photoconductor with a picosecond optical pulse [27]–[29]. The electrical signal on a line can then be sampled by electro-optic (EO) or photoconductive (PC) sampling. Some results for a GaAs FET mounted in a silicon-on-sapphire test circuit have been presented using this approach with PC sampling [30]. A comparison of this technique with frequency-domain measurements performed on a *Ka*-band integrated circuit has been made with an on-wafer characterization emphasis [31].

In the optoelectronic characterization of MMIC's, it is clearly advantageous to be able to generate the characterization signal on the wafer with only dc bias required, thereby avoiding the difficult problem of launching the microwave or millimeter-wave signal. This is where our technique differs from that reported in [26]. Whether one should use PC or EO sampling is an issue which warrants further consideration. Factors involved in making this choice are versatility (EO sampling can be performed anywhere), speed, sensitivity, ease of making the measurement, dynamic range, and accuracy.

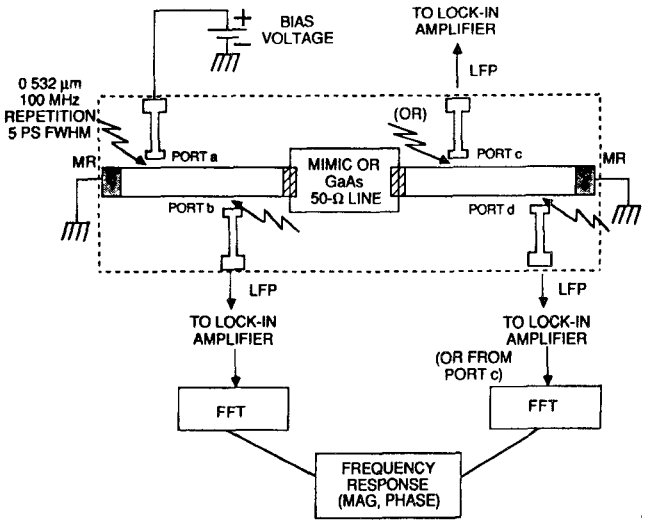

MR: MONOLITHIC RESISTOR OR MATCHED LOAD
LFP: LOW-FREQUENCY PROBE

Fig. 14. Schematic for optoelectronic measurement system using photoconductive sampling.

Upon a comparison of optoelectronic time-domain measurements with frequency-domain measurements, a number of trade-offs are evident. When measurements are performed in the time domain, broad-band information can be obtained with a single measurement. The bandwidth of the electrical signal generated using optoelectronic techniques can be tailored to a desired shape, which may be advantageous for some applications. The time-domain approach can be used to characterize nonlinear effects and the current optical technique can be simply extended for multiport measurements. It is clear that there are a number of issues which must be investigated to obtain a clear picture of the potential applications of optoelectronic time-domain techniques. Such techniques offer the possibility of measurement diversity, low-cost on-wafer probing, and broad-band characterization.

The measurement system for obtaining two-port scattering parameters using PC sampling is shown in Fig. 14. The pulse generation occurs at ports *a* or *d*, with the pulse traveling away from the device under test (DUT) either being terminated in the matched load or being windowed out by the sampling time duration. Photoconductive sampling is based on the small-signal operation of the photoconductor whereby the time-dependent portion of the sampled signal (as a function of the delay between the sampling and generation optical pulses) has been shown to correspond to the cross-correlation between the electrical signal on the line and the PC response of the sampling

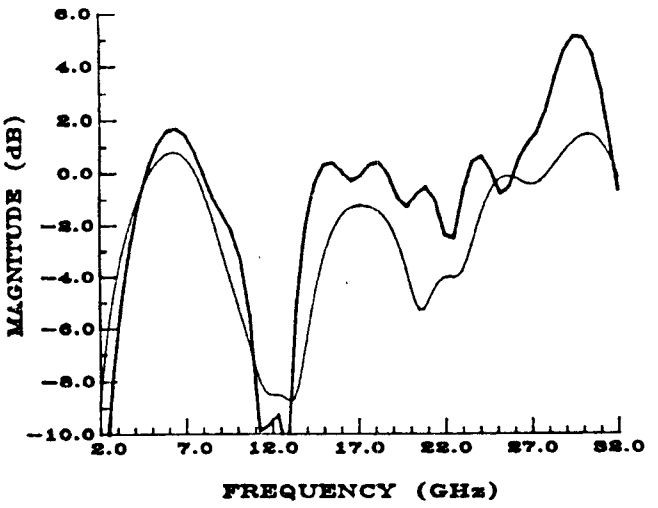

Fig. 15. S_{21} magnitude determined by EO sampling (light) and PC sampling (bold).

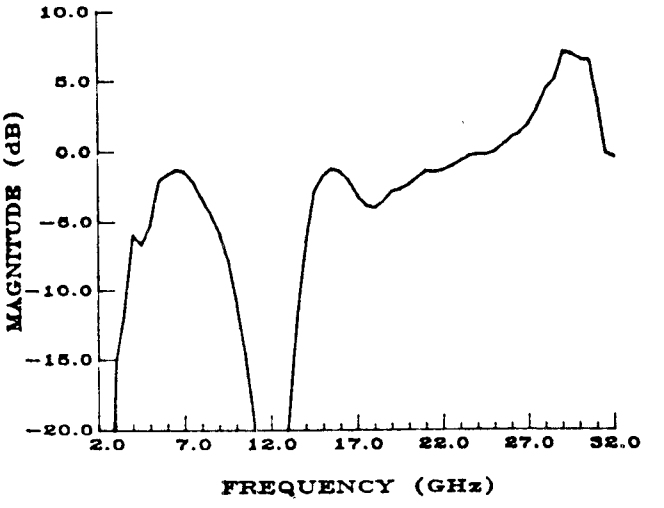

Fig. 16. S_{21} magnitude measured with network analyzer (HP8510)

gap, which is assumed to be identical to the generation gap [27]. If the DUT is assumed linear, then the broad-band scattering parameters can be reconstructed from the measured time-domain response by appropriately windowing the measured data at the sampling ports and using the fast Fourier transform (FFT).

The $S_{21}(f)$ and S_{11} of the DUT can be obtained by

$$S_{21}(f) = \frac{G_{ct}(f)}{G_{bi}(f)} \tag{8}$$

and

$$S_{11}(f) = \frac{G_{br}(f)}{G_{bi}(f)} \tag{9}$$

where $G_{bi}(f)$ is the Fourier transform of the sampled signal at input b for the incident signal and $G_{br}(f)$ for the reflected signal and $G_{ct}(f)$ is that of the transmitted signal sampled at port c.

If the sampling is to be performed using the EO effect, the probe signal can be located anywhere along the microstrip line, subject to the constraint of resolving the incident and reflected time-domain signals. The principle of operation relies on the electric field induced (due to electrical signal on the line) polarization rotation of the optical probe beam [26]. This approach of course relies on the use of either an EO substrate or a sampling probe. The detected sampled signal then follows the shape of the time-domain electrical signal on the line, so the scattering parameters can be obtained by simply forming a ratio of the Fourier transform of the windowed sample time-domain waveforms, representing the incident, reflected, and transmitted signals.

The implementation of both the PC and EO sampling of a 28 GHz MMIC and a comparison of the optical sampling results with those obtained by a conventional network analyzer measurement have been reported in [31] and [32]. The reader is referred to these papers for detail. Fig. 15 show the magnitude of S_{21} parameter measured by the EO and PC sampling techniques, and the corresponding data as determined by the network analyzer measurements (HP 8510) are shown in Fig. 16. In addition to the complete phase data of S_{21}, the measurement of both magnitude and phase of S_{11} has also been reported in [31] and [32]. The magnitude of S_{21} measured by the PC sampling technique agrees well with that obtained by the conventional network analyzer. The magnitude measured by the EO technique is low and may be due to calibration problems. The calibration is more difficult to obtain with EO sampling because the signal is very sensitive to the position of the sampling beam next to the microstrip line.

In comparing PC and EO methods, we found that it is more difficult to implement electro-optic sampling because of its lower sensitivity. For our device, the ratio of the detected signal voltage to the sampled voltage is 2×10^{-5} for electro-optic sampling and 3×10^{-3} for photoconductive sampling. This gives a dynamic range of 34 dB for EO sampling with the maximum voltage being the same, i.e., 300 mV. We have found that in the EO sampling there is also an interferometric effect between the front-surface-reflected beam and the beam reflected by the ground plate. It turns out that the EO signal magnitude also depends on the local wafer thickness if the coherent sampling pulse duration is longer than or comparable to the round-trip transit time through the wafer [33].

Although there is a good overall agreement in the broad-band response of the MMIC both in magnitude and phase measured by the PC sampling and the network analyzer techniques, we also note some discrepancies. These differences may be due to de-embedding. In the network analyzer measurement, the data were obtained by measuring the response of the package consisting of two photoconductive switches, the MMIC, and the K connectors. In order to compare these results with the optical techniques, it was necessary to correct for the loss and phase shift due to the 50 Ω line of the switches and the effect of the K connectors. This de-embedding process may introduce some errors into the network analyzer measurements. The effect of the K connectors is determined by measuring the S parameters for a separate test structure. Since the per-

formance of the K connectors is dependent upon the way the connectors are assembled, this term may be a source of error.

A CW measurement technique using picosecond optoelectronic sampling of GaAs microwave integrated circuits has been reported by the group at Stanford University [26]. The major difference between our technique and theirs is that we generate the input signal on the wafer, whereas their method requires that a CW microwave generated external to the wafer be launched into the circuit through a coplanar waveguide probe tip similar to that used in a commercial microwave probe station. As such ours is a pulse technique while theirs is a CW technique. A similar CW technique has been applied to characterize the performance of a packaged 1.7 GHz GaAs planar integrated decision circuit [34].

A picosecond switching time measurement of a resonant tunneling diode has been reported. Picosecond bistable operation has been experimentally observed in a double-barrier resonant tunneling diode [35]. A rise time of 2 ps has been measured. This time-domain measurement adds necessary information to the understanding of the transport mechanisms in the resonant tunneling diode.

The electro-optic sampling technique has also been applied for high-frequency characterization of thin-film high-temperature superconducting transmission lines [36]. Distortion-free propagation of high current density transient has been demonstrated. The high-frequency properties can be analyzed by careful study of the relative phase delays of the electrical transients as the temperature of the sample is varied to cover a wide temperature range, from 1.8 K to T_c [37].

VIII. Conclusion

In this paper I have reviewed the application of ultrafast optics technology to microwave and millimeter-wave technology. The link between these two technologies is picosecond optoelectronics, defined as an electronic function performed by ultrafast optical pulses of picosecond and/or femtosecond duration via the picosecond photoconductivity effect. This new technique provides perfect time synchronization and thus coherency between the optical and microwave events. Both CW and pulsed microwaves can be generated and controlled by optical techniques using a frozen wave generator, an impulse excited cavity resonator, or an optically controlled dielectric waveguide. A broadband on-wafer characterization technique has been discussed which essentially performs the time-domain network analysis for MMIC before the wafers are diced off. Since the optical and electronic events can be perfectly time synchronized, many interesting coherent measurement techniques have been invented. One aspect of recent work that has not been discussed in this paper concerns picosecond photoconducting dipolar antennas [38]–[40]. These structures are capable of generating and coherently detecting picosecond and subpicosecond electric pulses. These antennas, when illuminated with femtosecond optical pulses, radiate electrical pulses with frequency spectra extending from dc to THz. Possible applications of this technique include the characterization of microwave materials. The coherent technique allows independent determination of both the real and imaginary parts of the dielectric constant [41].

In conclusion, we have seen many interesting new developments of using ultrafast optics in microwave technology. In the future, as the technique is perfected and technology matures, we can foresee some merging of ultrafast optics and microwaves.

Acknowledgment

The author would like to acknowledge technical contributions from D. Butler, C. S. Chang, E. A. Chauchard, R. Fischer, H. L. A. Hung, M. G. Li, P. Polark-Dingels, M. J. Rhee, A. Rosen, H. A. Sayadian, and K. J. Webb.

References

[1] H W. Yen, M. K Barnoski, R. G. Hansperger, and R. T. Melville, "Switching to GaAs IMPATT diode oscillator by optical illumination," *Appl Phys Lett*, vol 31, pp. 120–122, July 1977.

[2] J. R. Forrest and A J. Seeds, "Optical control of IMPATT microwave oscillators," in *1978 IEEE Int Electron Device Meeting Tech. Dig*, Dec. 1978, pp 282–285.

[3] Horst W. A. Gerlach and R. Wellman, "The behavior of a pulsed millimeter-wave (70 GHz) IMPATT diode oscillator during laser illumination" in *1980 IEEE MTT-S Int. Microwave Symp Dig.*, May 1980, pp 70–72.

[4] R A Keihl, "Behavior and dynamics of optically controlled TRAPATT oscillators," *IEEE Trans. Electron Devices*, vol. ED-25, pp 703–710, June 1978

[5] A A. A. DeSalles, "Optical control of GaAs MESFET's," *IEEE Trans Microwave Theory Tech.*, vol. MTT-31, pp. 812–820, Oct. 1983

[6] R N Simons and K B. Bhasin, "Analysis of optically controlled microwave/millimeter wave device structures," in *1986 IEEE MTT-S Int. Microwave Symp. Dig*, June 1986, pp. 551–554

[7] T F Carruthers, "Picosecond optical control of transferred-electron devices," in *Picosecond Optoelectronic Devices*, C H. Lee, Ed. New York: Academic Press, 1984, pp 339–371

[8] R. N Simons and K. B. Bhasin, "Microwave performance of an optically controlled AlGaAs/GaAs high electron mobility transistor and GaAs MESFET," in *IEEE MTT-S Int Microwave Symp. Dig.*, June 1987, pp. 815–818.

[9] L Goldberg, A. M Yurek, H. F Taylor, and J. F Weller, "35 GHz microwave signal generation with an injection locked laser diode," *Electron Lett.*, vol. 21, pp. 814–816, 1985.

[10] A. S. Daryoush, P. R. Herczfeld, A. Rosen, A. K. Sharma, and V M. Contarino, "Indirect subharmonic optical injection locking of millimeter-wave IMPATT oscillator," in *1986 IEEE MTT-S Int Microwave Symp. Dig*, 1986, pp 109–112.

[11] T Berceli, A. S Daryoush, P. R Herczfeld, W. D. Jemison, and A Paolella, "A MMIC based injection locked oscillator for optically fed phased array antennas," in *IEEE MTT-S Int. Microwave Symp. Dig*, June 1989, pp. 131–134.

[12] S. Jayaraman and C. H. Lee, "Observation of two-photon conductivity in GaAs with nanosecond and picosecond light pulse," *Appl. Phys Lett*, vol. 20, pp 392–395, 1972

[13] M. B. Ketchen *et al.*, "Generation of subpicosecond electrical pulses on coplanar transmission lines," *Appl Phys. Lett.*, vol. 48, pp 751–753, 1986

[14] H. A. Sayadian, M.-G Li, and Chi. H Lee, "Generation of high-power broad-band microwave pulses by picosecond optoelectronic technique," *IEEE Trans. Microwave Theory Tech*, vol 37, pp. 43–50, 1989

[15] D. Butler *et al.*, "A cw 20-GHz opto-electronic source with phased-array applications," *Microwave and Opt. Technol. Lett.*, vol. 1, pp. 119–123, 1988.

[16] F. W. Smith *et al*, "Picosecond GaAs based photoconductive optoelectronic detectors," *Appl. Phys. Lett*, vol. 54, pp 890–892, 1989

[17] M. C. Nuss, D. W Kisker, P. R. Smith, and T. E. Harvey, "Efficient generation of 480 fs electrical pulses on transmission lines by photoconductive switching in metalorganic chemical vapor deposited CdTe," *Appl. Phys. Lett.*, vol. 54, pp. 57–59, 1989.

[18] Chi H. Lee, P. S Mak, and A. P. DeFonzo, "Optical control of millimeter-wave propagation in dielectric waveguides," *IEEE J. Quantum Electron*, vol. QE-16, pp. 277–288, 1980.

[19] A. M. Yurek, C D. Striffer, and Chi H. Lee, "Optoelectronic devices for millimeter-waves," in *Infrared and Millimeter-Wave*, vol. 14, *Millimeter Components and Techniques*, K. J. Button, Ed. Orlando, FL: Academic Press, 1985.

[20] D. Krokel, D. Grischkowsky, and M. B. Ketchen, "Subpicosecond electric pulse generation using photoconductive switches with long carrier lifetimes," *Appl. Phys. Lett.*, vol. 54, pp. 1046–1047, 1989.

[21] G. M. Loubriel, M. W. O'Mally, and F. J Zutavern, "Toward pulsed power uses for photoconductive semiconductor switches: closing switches," in *Proc. 6th IEEE Pulsed Power Conf.*, 1987, pp. 145–148.

[22] H. M. Cronson, "Picosecond-pulse sequential waveform generation," *IEEE Trans. Microwave Theory Tech.*, vol. MTT-23, pp. 1048–1049, 1975.

[23] J. M. Proud, Jr., and S. L. Norman, "High-frequency waveform generation using optoelectronic switching in silicon," *IEEE Trans. Microwave Theory Tech.*, vol. MTT-26, pp. 137–140, 1978.

[24] C. S. Chang, M. J. Rhee, Chi H. Lee, A. Rosen, and H. Davis, "Kilovolt sequential waveform generation by picosecond optoelectronic switching in silicon," in *Picosecond Electronics and Optoelectronics*, G. A. Mourou, D. M. Bloom, and Chi H. Lee, Eds. New York: Springer-Verlag, 1985, pp. 220–223

[25] A. Rosen, P. J. Stabile, A. K. Sharma, Chi H. Lee, and P. Polak-Dingels, "Direct dc-to-rf conversion by impulse excitation utilizing a lateral pin diode as a switch," *Microwave and Opt. Technol. Lett.*, vol 1, pp. 106–110, 1988.

[26] K. J. Weingarten, M J. Rodwell, and D M Bloom, "Picosecond optical sampling of GaAs integrated circuits," *IEEE J. Quantum Electron.*, vol. 24, pp. 198–220, 1988.

[27] D. H. Auston, "Picosecond photoconductors: Physical properties and applications," in *Picosecond Optoelectronic Devices*, Chi H. Lee, Ed. Orlando, FL: Academic, 1984.

[28] D. H. Auston, "Impulse response of photoconductor in transmission lines," *IEEE J Quantum Electron.*, vol. QE-19, pp. 639–648, 1983.

[29] Chi H. Lee, Ed , *Picosecond Optoelectronic Devices*. Orlando, FL: Academic Press, 1984

[30] D. E. Cooper and S. C. Moss, "Picosecond optoelectronic measurement of the high frequency scattering parameters of a GaAs FET," *IEEE J. Quantum Electron.*, vol. QE-22, pp. 94–100, 1986.

[31] H. L. A. Hung *et al.*, "Millimeter-wave monolithic integrated circuit characterization by a picosecond optoelectronic technique," *IEEE Trans. Microwave Theory Tech.*, vol. 37, pp. 1223–1231, 1989.

[32] K J Webb *et al.*, "A time domain network analyzer which uses optoelectronic technique," in *1989 IEEE MTT-S Int. Microwave Symp. Dig.*, vol. 1, pp 220.

[33] M. G. Li, E. A. Chauchard, and Chi H. Lee, "New approach to detection of electrooptic affect in GaAs circuits," in *Proc. OSA Annual Meetings* (Orlando), 1989, paper Th T5.

[34] M. S. Heutmaker, T. B. Cook, B. Bosacchi, J. M. Wiesenfeld, and R. S. Tucker, "Electrooptic sampling of a packaged high speed GaAs integrated circuit," *IEEE J Quantum Electron.* vol. 24, pp. 226–233, 1988.

[35] J. F. Whitaker, G. A. Mourou, T. C. L. G. Sollner, and W D. Goodhue, "Picosecond switching time measurement of a resonant tunneling diode," *Appl. Phys. Lett.*, pp. 385–387, 1988.

[36] D. R. Dykaar *et al.*, "High-frequency characterization of thin-film Y-Ba-Cu oxide superconducting transmission lines," *Appl. Phys. Lett.*, pp. 1444–1446, 1988.

[37] M. Nuss *et al.*, "Propagation of terahertz bandwidth electrical pulses on $YBa_2Cu_3O_7$ transmission lines on lanthanum aluminate," *Appl Phys. Lett.*, vol. 54, pp. 2265–2267, 1989.

[38] A P. DeFonzo and C R. Lutz, "Optoelectronic transmission and reception of ultrashort electrical pulses," *Appl. Phys. Lett* , vol. 51, pp. 212–214, 1987.

[39] P R. Smith, D. H. Auston, and M. C. Nuss, "Subpicosecond photoconductive dipole antennas," *IEEE J. Quantum Electron.*, vol. 24, pp. 255–260, 1988.

[40] M. V. Exter, Ch Fattinger, and D. Grischkowsky, "High-brightness terahertz beams characterized with an ultrafast detector," *Appl. Phys. Lett.*, vol. 55, pp. 337–339, 1989.

[41] G. Arjavalingam, Y. Pastol, J.-M. Halbout, and G. V. Kopcsay, "Broad-band microwave measurements with transient radiation from optoelectronically pulsed antennas," pp 615–621, this issue.

✠

Chi H. Lee (M'80–SM'86) received the B.S. degree in electrical engineering from National Taiwan University, Taipei, Taiwan, in 1959 and the M.S. and Ph.D. degrees in applied physics from Harvard University, Cambridge, MA, in 1962 and 1968 respectively.

He was with the IBM San Jose Research Laboratory from 1967 to 1968. Since 1968 he has been with the University of Maryland, College Park, where he is now a Professor of Electrical Engineering. His areas of research include picosecond optoelectronics, lasers, optical techniques for microwave application, and millimeter-wave devices.

Dr. Lee is a Fellow of the Optical Society of America and a member of the American Physical Society. He also served as Chairman of the IEEE MTT-S Technical Committee for Lightwave Technology.